How Does the Winter Jet Stream Affect Surface Temperature, Heat Flux, and Sea Ice in the North Atlantic?

LIPING MA

School of Environmental Sciences, University of Liverpool, Liverpool, United Kingdom

TIM WOOLLINGS

Department of Physics, University of Oxford, Oxford, United Kingdom

RICHARD G. WILLIAMS

School of Environmental Sciences, University of Liverpool, Liverpool, United Kingdom

DOUG SMITH AND NICK DUNSTONE

Met Office, Hadley Centre, Exeter, United Kingdom

ABSTRACT

The role of the atmospheric jet stream in driving patterns of surface heat flux, changes in sea surface temperature, and sea ice fraction is explored for the winter North Atlantic. Seasonal time-scale ensemble hindcasts from the Met Office Hadley Centre are analyzed for each winter from 1980 to 2014, which for each year includes 40 ensemble members initialized at the start of November. The spread between ensemble members that develops during a season is interpreted to represent the ocean response to stochastic atmospheric variability. The seasonal coupling between the winter atmosphere and the ocean over much of the North Atlantic reveals anomalies in surface heat loss driving anomalies in the tendency of sea surface temperature. The atmospheric jet, defined either by its speed or latitude, strongly controls the winter pattern of air–sea latent and sensible heat flux anomalies, and subsequent sea surface temperature anomalies. On time scales of several months, the effect of jet speed is more pronounced than that of jet latitude on the surface ocean response, although the effect of jet latitude is important in altering the extent of the ocean subtropical and subpolar gyres. A strong jet or high jet latitude increases sea ice fraction over the Labrador Sea due to the enhanced transport of cold air from west Greenland, while sea ice fraction decreases along the east side of Greenland due either to warm air advection or a strong northerly wind along the east Greenland coast blowing surface ice away from the Fram Strait.

1. Introduction

Midlatitude atmospheric variability is known to strongly influence the underlying ocean, in particular by modulating surface heat fluxes and wind-induced Ekman circulations. The atmospheric influence on the North Atlantic Ocean is often viewed in terms of the North Atlantic Oscillation (NAO), which is strongly associated with a tripole pattern in sea surface temperatures (Bjerknes 1964; Visbeck et al. 2003; Marshall et al. 2001a; Eden and Willebrand 2001). The imprint of this atmospheric forcing associated with the NAO involves both local and far-field responses affecting the ocean heat storage over the North Atlantic. Anomalies in air–sea heat flux drive convection and interannual changes in local heat content over the subpolar gyre (Visbeck et al. 2003; Grist et al. 2010), while changes in wind stress drive variations in subtropical heat content (Lozier et al. 2008; Williams et al. 2014) and intergyre transfers between the subtropical and subpolar gyres (Marshall et al. 2001b). The combined effect of wind stress and air–sea

---

Corresponding author: Liping Ma, liping.ma@liverpool.ac.uk

buoyancy flux changes drive variations in the meridional overturning (Lozier et al. 2010; Robson et al. 2012), which in turn alters the gyre-scale convergence in heat transport (Williams et al. 2014; R. G. Williams et al. 2015) and controls multiyear and decadal changes in ocean heat content.

The NAO is a statistical measure for the state of the atmosphere and is typically defined from the mean sea level pressure using principal component analysis or a simple point difference (Hurrell and Deser 2010). As such, the NAO only empirically relates to the underlying atmospheric phenomena and may be affected by any circulation that projects onto its spatial pattern (Johnson et al. 2008). However, the majority of the variance of the NAO is known to represent variations of the North Atlantic eddy-driven jet stream (Thompson et al. 2003). Changes in both the strength and the latitude of the jet project onto the NAO, so that a positive NAO may indicate a strengthening, or a northward shift of the jet, or both (Woollings et al. 2010). The implications of the NAO and other weather regimes, including atmospheric blocking, on the surface ocean have been investigated using nonlinear, regime-based methods (Cassou et al. 2004, 2011; Barrier et al. 2014).

Although combined in the NAO, there is evidence that the strength and position of the jet are physically distinct structures of variability, for example having quite different seasonal cycles and power spectra, and they are generally uncorrelated in terms of interannual variability (Woollings et al. 2014). In addition, idealized models suggest that the jet indices have different sensitivities, for example with the jet latitude responding most strongly to local heating on either side of the jet maximum, while the jet speed is sensitive to heating in the deep tropics (Baker et al. 2017). These differing sensitivities can largely be understood as reflecting changes in the strength or location of the maximum meridional temperature gradient, which can affect the growth of baroclinic eddies. The variance of jet latitude appears to be modulated by the jet speed on decadal time scales (Woollings et al. 2018) with potential implications for ocean decadal variability (Czaja 2009; Häkkinen et al. 2011).

The aim of this paper is therefore to revisit the influence of atmospheric variability on the surface North Atlantic Ocean from the jet stream perspective, treating the jet position and strength separately. The position and strength of the eddy-driven jet are identified using jet indices based on the maximum of the zonally averaged zonal wind (Woollings et al. 2018). These jet indices are relatively simple, neglecting for example the meridional tilt of the jet (Madonna et al. 2017), but have the advantage of providing simple time series comparable to

the NAO. The jet indices explain much of the variability associated with both the NAO and the east Atlantic (EA) pattern (Woollings et al. 2010), that is, the two leading empirical orthogonal functions (EOFs) in the region, but not that associated with higher-order EOFs such as the Scandinavian pattern. An additional motivation for this separation is that the NAO seems to reflect a different balance of the two jet indices on different time scales, with the jet latitude dominating on interannual time scales, but the jet speed becoming more important on multidecadal time scales (Woollings et al. 2015).

Atlantic multidecadal variability has considerable regional climate impact (Knight et al. 2006; Sutton and Dong 2012) with the ocean playing an important role in this variability (Gulev et al. 2013; O'Reilly et al. 2016). Climate models generally underestimate multidecadal variability in both the ocean and the atmosphere (Kravtsov 2017; Kim et al. 2018; Simpson et al. 2018), in particular in the speed of the jet rather than its latitude (Bracegirdle et al. 2018). Hence the differing effects of jet latitude and speed on the ocean may be of importance for understanding Atlantic multidecadal variability.

Analyses of ocean–atmosphere coupling in observations have limited ability to identify causal relationships due to the several different mechanisms operating on different time scales between the ocean, the local atmosphere and potential remote drivers. Hence, although we do make some comparison with reanalysis data in this paper, the majority of our analysis focuses on a large ensemble of historical model simulations, in which inferences of causality are less problematic. For each season we compare the evolution of forty individual ensemble members, each initialized with identical ocean states and small perturbations in the atmosphere. Our primary assumption is that the spread in ocean variables between ensemble members over the following few months is determined by their different realizations of chaotic atmospheric variability. Analysis across the ensembles allows the sensitivity of the ocean to jet latitude and jet speed to be identified. One caveat to this approach is that sensitivities are only considered on monthly to seasonal time scales, so do not include delayed responses that may be important in explaining decadal changes in surface warming (Robson et al. 2012). Heat loss from the ocean to the atmosphere is often strongly modulated by synoptic time-scale processes, such as midlatitude cyclones (Parfitt and Seo 2018) and the related cold air outbreaks (Papritz and Spengler 2017; Vannière et al. 2017). These events are themselves modulated by low-frequency variability of the large-scale flow (Kolstad et al. 2009; Woollings et al. 2016).

In this paper, we focus on the seasonal evolution of the coupled system and hence we investigate the role of the

large-scale circulation, following studies such as Visbeck et al. (2003), Zhai et al. (2004), and Cassou et al. (2011). We use indices of the eddy-driven jet stream derived from the lower-tropospheric zonal winds that provide direct measures of a time-averaged wind, as well as act to integrate the effects of the transient weather systems that drive the jet (Hoskins et al. 1983). Despite the importance of synoptic- and smaller-scale processes, we show that large fractions of the variance in surface heat flux on seasonal time scales can be accounted for by the flow variations summarized by these two simple jet indices.

2. Methods and data

Seasonal hindcasts are analyzed from the Met Office Decadal Prediction System, version 3 (DePreSys3) (Smith and Murphy 2007; Smith et al. 2007; Dunstone et al. 2016), designed to make global and regional climate predictions over seasonal to decadal time scales. DePreSys3 is based on the HadGEM3-GC2 coupled climate model (K. Williams et al. 2015) with an atmospheric horizontal resolution of $0.83° \times 0.55°$. Hindcasts are initialized using the 1 November conditions provided by the assimilation run from years 1980 to 2014: 40 different ensemble members are initialized with the same ocean and sea ice state from the assimilation run and only differ in the atmosphere by random seeds supplied to a stochastic physics scheme. An ensemble is created by providing different seeds to a stochastic physics scheme (Bowler et al. 2009). This model dataset then comprises 40 ensembles over each month of the 35 years (hereafter named ensemble data). The model analysis is also compared with ERA-Interim reanalysis monthly and daily data from the same period from 1980 to 2014.

In this study, surface latent heat flux, sensible heat flux, sea surface temperature, air temperature at 1.5 m in ensemble data and 2 m in reanalysis daily data, sea ice fraction, 850-hPa zonal wind, and 10-m winds for the ensemble and monthly and daily reanalysis datasets from years 1980 to 2014 are employed. In the ensemble data, surface temperature is defined by the temperature of the surface land and ice where they occur, and elsewhere represent sea surface temperature; so that in polar regions, surface temperature may reach from $-30°$ to $-40°$C.

a. Jet structure in the ensemble hindcast dataset

The speed and latitude of the atmospheric jet stream are defined by the maximum value of the monthly mean zonal wind at 850 hPa averaged longitudinally over the North Atlantic sector (60°W–0°) (Woollings et al. 2010). In the ensemble data, there are 4200 separate ensembles made up of 40 ensemble members per month for each of
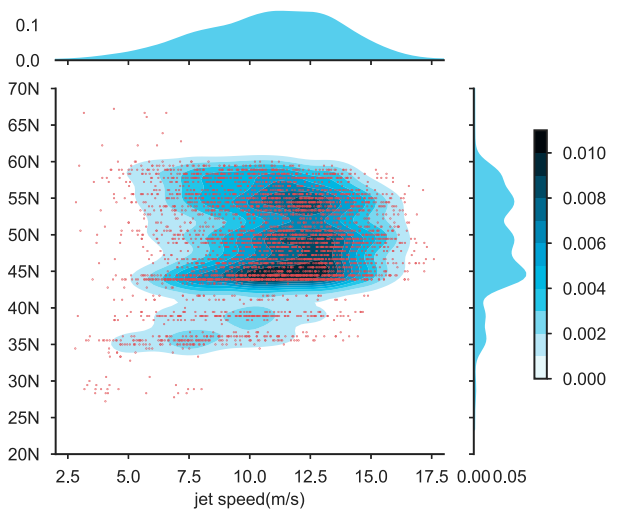

FIG. 1. Jet stream speed vs latitude density distribution structure in wintertime (December–February) 1980–2014 over the North Atlantic based on the ensemble monthly data. Colored contours represent the density (i.e., the number of points per 0.55°N degree bin × m s⁻¹ speed in 0.55°N m s⁻¹). The top graph represents the probability density of jet speed; the right graph represents the probability density of jet latitude. The probability density of the jet is mapped using a kernel density estimation where each speed vs latitude point is identified and the density of points is shown as the number of points per 0.55°N m s⁻¹.

the three winter months, and repeated over 35 years (Fig. 1). There is a trimodal latitudinal structure for the jet with frequent occurrences at 45°, 49°, and 55°N for the winter period Decembe–February (Fig. 1), as well as a relatively weak occurrence at 35°N. These monthly distributions with a trimodal latitudinal distribution are similar to daily analyses based on reanalysis data (Woollings et al. 2018 for a similar daily figure). Comparison of the ensemble model monthly and reanalysis daily and monthly data distributions (not shown) reveals that the ensemble model generally captures the observed distribution of weather time-scale jet variability well, and so the ensemble monthly data are a suitable tool to investigate the impacts of jet variability on the underlying ocean.

In both the ensemble data and the reanalysis datasets, the jet latitude and speed are not linearly correlated, and represent two physically distinct pieces of information on the jet. Analysis of the ensemble data reveals a strong relationship between the jet indices and NAO index during wintertime (December–February) with the strength of the jet associated with a positive NAO with a 0.72 correlation coefficient, while the jet latitude is associated with a positive NAO with a 0.57 correlation coefficient. Hence, a positive NAO may indicate a strengthening, or a northward shift of the jet, or both (Woollings et al. 2010).

b. Ensemble sensitivity analysis

One of our aims is to explore the causality operating between the atmosphere and ocean by applying an ensemble sensitivity analysis to the hindcast data (following a similar method to Torn et al. 2015). The ensemble sensitivity analysis is based on analysis of the spread in the evolution of the ensemble members from their similar initial state. While there may be a systematic evolution common to the members, representing an underlying dynamical control or possibly a systematic effect of the ocean, the divergence of the ensembles on the seasonal time scale largely represents the effects of stochastic processes originating in the atmosphere.

The sensitivity of an outcome J to a precursor variable x is evaluated from the covariance of J and x, which may represent the air–sea heat flux and jet speed, respectively. The normalized sensitivity is defined by the ratio of the covariance and the standard deviation of the precursor:

$$\frac{\partial J}{\partial x} = \frac{\text{cov}\{J, x\}}{\text{std}\{x\}}, \tag{1}$$

where the normalization has provided units of J per standard deviation of x across the ensembles.

For ensemble sensitivity analyses, a two-stage process is applied to assess correlations between variables in the ensembles: (i) the correlation between jet indices and surface ocean variables across the 40 ensemble members for each winter month in each individual year of the 35 years is evaluated, for instance, the correlation between January jet indices and February sea surface temperature is calculated across 40 ensembles in each year, so that there are 40 samples for each year's correlation calculation (rather than the 1400 samples of the entire dataset), as a result, there are 35 correlation maps created; and (ii) a mean is then taken over these 35 maps to provide a climatological mean map. In addition, to assess their significance, a t test is employed using the 40 samples, where each ensemble is taken to be independent. The correlation passes statistical significance tests with confidence levels of 90% at ± 0.26, 95% at ± 0.31, and 99% at ± 0.40.

3. The effect of the atmospheric jet on the surface wind and air temperature advection

In this section, the effects of the atmospheric jet speed and latitude are explored on the ocean surface wind patterns, and the wind-induced Ekman horizontal and vertical transport are evaluated; also the air temperature advection $-\mathbf{v} \cdot \nabla T_a$ is estimated from the 10-m wind and air temperature at 1.5 m in ensemble data and 2 m in reanalysis daily data.

To highlight this dependence on the jet indices, we consider the pattern and strength of the surface wind fields and air temperature advection from the ensemble data by comparing ensembles for the top 200 high and low jet indices in a composite analysis. The 200 highest and 200 lowest jet indices ensembles are chosen across the years 1980–2014 in the same months. The ensemble model data reveals many more extreme events, in particular in terms of weak cases for the jet speed compared with the reanalysis data (Fig. 1). In our analysis of the ensemble data, very weak jet speed events that are lower than $5\,\mathrm{m\,s^{-1}}$ are excluded so that the 200 lowest jet speed cases range in strength from 5 to $8.7\,\mathrm{m\,s^{-1}}$, while the jet highest speed events range in strength from 17.5 to $14\,\mathrm{m\,s^{-1}}$. For the jet latitude ranges, the 200 highest jet latitude cases extending between 56° and 66°N are considered and those events higher than 66°N are excluded, while the lowest 200 jet latitude cases extend between 30° and 43°N and events below 30°N are excluded.

For a composite of the strong jet cases, a strong jet brings cold air from west Greenland and Baffin Bay or the North American continent down to the south Greenland Sea and subpolar gyre, with cold air advection reaching over $-10\,\mathrm{K\,day^{-1}}$ over the boundaries (Fig. 2a). On the other hand relatively warm air is transported from the subtropics from 30° to 40°N with warm air advection reaching over 1–$2\,\mathrm{K\,day^{-1}}$ directed northeastward to the British Isles then transported cyclonically over the Nordic seas and eventually meets cold air from north Greenland. By contrast, in a composite of the 200 weakest jet cases, the surface westerly wind is fairly weak and tilts southwest–northeast over most of the midlatitudes, and leads to warm air advection from the subtropics up to the south of Iceland and the region north of Iceland is dominated by a cold northerly wind from the Arctic (Fig. 2b). For a composite of high jet latitude, the central Atlantic warm air about $3\,\mathrm{K\,day^{-1}}$ is transported farther north but not as far as the Nordic seas and cold air is constrained to a narrower region around the south of Greenland (Fig. 2c). In a composite of the low-latitude cases, the warm air temperature advection is spread over a wider area limiting the spread of the cold air (Fig. 2d). Finally, the differences in both the wind fields and air temperature advection between high and low jet speed states reveal that a strong jet enhances warm air advection by 1–$3\,\mathrm{K\,day^{-1}}$ to the north and east Iceland and the cold air advection anomalies are from around -1 to $-4\,\mathrm{K\,day^{-1}}$ over the most of the subpolar region (Fig. 2e). The difference anomalies between high and low jet latitude show similar patterns but are shifted farther north (Fig. 2f).

Repeating the composite analysis for the differences in the wind patterns and air temperature advection
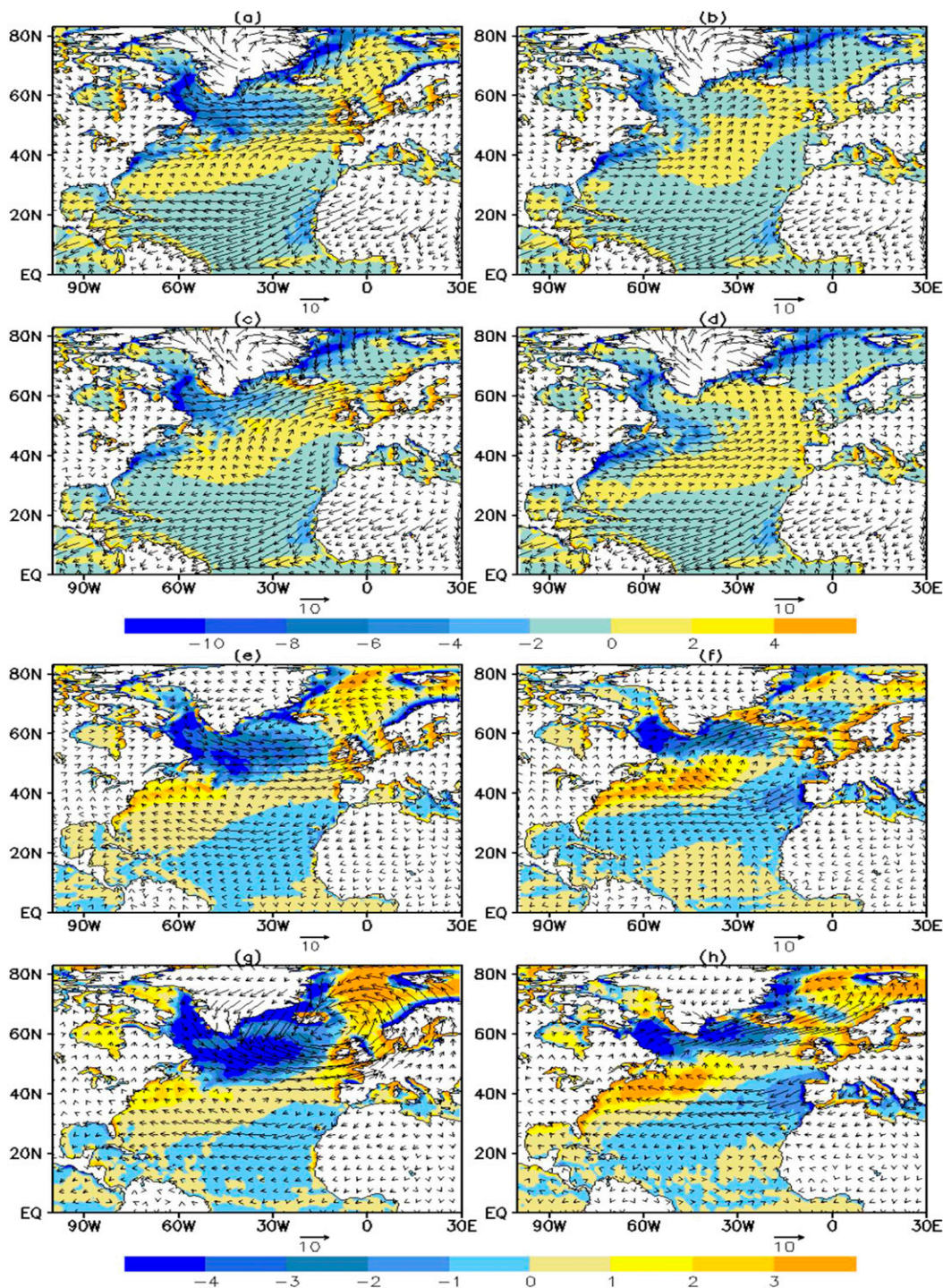
FIG. 2. A composite mean of 200 January months from ensemble data of 10-m wind (vectors; m s^{-1}) and air temperature advection (shading; K day^{-1}; calculated from 10-m wind and 1.5-m air temperature) during (a) high jet speed state, (b) low jet speed state, (c) high jet latitude state, and (d) low jet latitude state; the differences in 10-m wind and air temperature advection between a composite of 200 January months of (e) the highest jet speed minus that for the lowest jet speed and (f) the highest jet latitude minus that for the lowest jet latitude; the differences in 10-m wind and air temperature advection (calculated from 10-m wind and 2-m air temperature) from reanalysis daily data between a composite of 200 January days of (g) the highest jet speed minus that for the lowest jet speed and (h) the highest jet latitude minus that for the lowest jet latitude.

associated with jet strength and position for daily re-analysis data (Figs. 2g,h) reveals similar patterns as the monthly fields from the ensemble (Figs. 2e,f) and the reanalysis (not shown). Note that the anomaly magnitudes are slightly larger in the daily data, as the variations in the jet indices are larger in the daily data. This larger range is especially true for the high jet speed events, which are in the range 19–25 m s^{-1} in the daily data, so that the range in jet speed in the composite is increased by 60%. There are also some detailed differences with more prominent northerly and north-westerly winds in daily fields associated with a strong jet along east Greenland and the Labrador Sea (Fig. 2g). These differences may reflect the greater importance of meridional wind on the daily time scale, as highlighted by Ogawa and Spengler (2019), who raised the concern that monthly analyses might be misleading as a result. However, our synoptic time-scale analysis suggests that this is a minor effect for the jet indices. In a similar manner, the impacts of jet latitude on wind direction and air temperature advection patterns based on daily reanalysis data are very similar to the ensemble monthly fields.

For the strong jet state, the magnitude of Ekman upwelling and downwelling velocities from the ensemble data are enhanced over most of the subpolar and subtropical region, reaching over 4×10^{-5} m s^{-1} and around -2×10^{-5} m s^{-1}, respectively (Fig. 3a). Meanwhile, Ekman southward volume transport is enhanced reaching -3 m^2 s^{-1} over most of the subpolar due to a strong westerly wind, whereas the northward Ekman transport is enhanced too due to an enhanced trade wind.

However, the pattern of Ekman volume transport and upwelling for the composites of the 200 highest jet latitude cases shift farther north than their counterparts during the 200 highest speed cases (Fig. 3c). For the 200 lowest jet latitude states, the Ekman transport and vertical velocity patterns are shifted farther south (Fig. 3d). Ekman upwelling is driven by cyclonic circulation or low pressure center and downwelling is driven by anticyclonic circulation or high pressure center. Thus, the strong jet enhances cyclonic circulation over Iceland and anticyclonic circulation over the Azores, while the northward-shifted jet shifts both cyclonic and anticyclonic circulation northward.

Overall, the jet stream strength and latitude change surface atmospheric circulation, and in turn alter zonal and meridional transport of cold and warm air.

4. The surface temperature response to heat flux anomalies

Before exploring the links between jet stream and ocean variability, the connection between the surface temperatures and heat fluxes are examined in the ensemble datasets, as their interaction is crucial in determining the influence of the atmosphere on the ocean.

For the surface air–sea fluxes, the latent and sensible heat fluxes, F_l and F_s, are related to the wind speed and the difference in the specific humidity and temperature, respectively, between the sea surface and the air in the boundary layer through bulk aerodynamic formulas (Cayan 1992; Isemer and Hasse 1987):

$$F_l = \rho L C_E u(q_s - q_a), \qquad (2)$$

$$F_s = \rho C_p C_H u(T_s - T_a), \qquad (3)$$

where u, q_a, and T_a are the wind speed, specific humidity, and temperature of the air in the boundary layer, respectively; and q_s and T_s are the saturation specific humidity and surface temperature, respectively; ρ is air density; L is the latent heat of evaporation; C_p is the specific heat capacity of air at constant pressure; and C_E and C_H are transfer coefficients for latent heat and sensible heat, respectively. In this study, a positive flux represents an ocean loss of heat.

a. The effect of surface heat flux on surface temperature

The anomalies in the surface heat flux are taken as the sum of anomalies in surface sensible and latent heat flux and are now correlated with both the surface temperature anomaly and its tendency. The tendency of surface temperature is defined based upon the surface temperature difference of the months before and after the central month, such as February minus December, following Cayan (1992). To assess the role of the atmosphere in driving sea surface temperature variability, we consider a local heat balance connects the anomalies in the tendency in surface temperature and the air–sea heat flux:

$$\frac{\partial T'_{sst}}{\partial t} = -\frac{1}{\rho C_p} \frac{F'}{h}, \qquad (4)$$

where F' is the total air–sea heat flux anomaly that is taken to be the sum of the latent and sensible heat flux anomalies (defined as positive when out of the ocean), h is the thickness of the mixed layer, and the prime represents a deviation from a time mean. Sea surface temperature variability is also driven by horizontal and vertical advection and mixing, such as involving instability of boundary currents and jets.

The mean correlation of the surface heat flux anomaly and tendency of sea surface temperature anomalies reveals the expected local heat balance holding over most of the North Atlantic, where greater surface heat loss drives a reduction in surface temperature: the heat flux
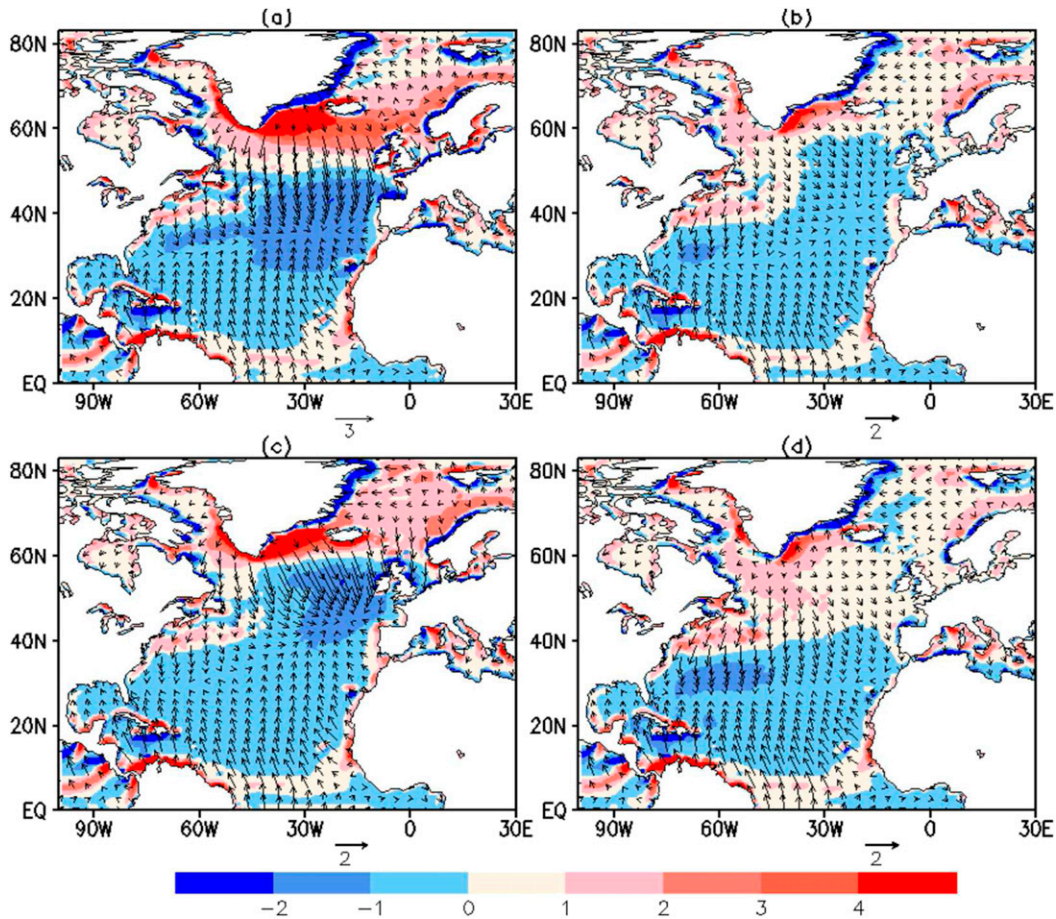
FIG. 3. A composite mean of 200 January months from ensemble data of Ekman horizontal volume transport (vectors; $m^2 s^{-1}$) and Ekman upwelling velocity (shaded color; $10^{-5} m s^{-1}$; the positive means upwelling, the negative means downwelling) during (a) high jet speed state, (b) low jet speed state, (c) high jet latitude state, and (d) low jet latitude state.

generally correlates well with the negative tendency in surface temperature anomaly for the same month, but not for the subsequent month (Figs. 4a,c). This relationship leads to the heat flux in January correlating more strongly with the temperature anomaly in February, rather than in January (Figs. 4b,d). However, this local heat balance does not hold over the Gulf Stream, where the advection of heat becomes important in controlling the surface temperature evolution (Figs. 4a,d) (Roberts et al. 2017).

The heat flux anomalies are weakly connected to surface temperature anomalies for the same month over most of the domain (Fig. 4b), although there is a positive correlation over the Gulf Stream suggesting air–sea heat fluxes respond to the advection of warm ocean anomalies (Roberts et al. 2017). Overall, the strong effect of heat flux on temperature tendency (Fig. 4a) leads to a clear impact on sea surface temperature in the following month (Fig. 4d).

b. The effect of surface heat flux on sea ice extent

The relationship between surface heat flux and sea ice extent is now considered due to their effect on the signals along the ocean boundaries in Fig. 4.

There are two different regimes with a dipole pattern exhibiting different responses for the connection between sea ice cover and air–sea heat flux (Fig. 5a) east of Greenland toward the Nordic seas and west of Greenland in the Labrador Sea.

Over the Labrador Sea, there is a positive correlation between January heat flux and January sea ice fraction, reaching 0.4–0.55 (Fig. 5a), implying that more heat loss is associated with more sea ice formation. This response is consistent with the expected negative correlation between anomalies in air–sea heat flux and surface temperature tendency (Figs. 4a,b,d), which involves surface cold air coming from upstream (see Fig. 2), cooling the ocean surface and encouraging sea ice formation.
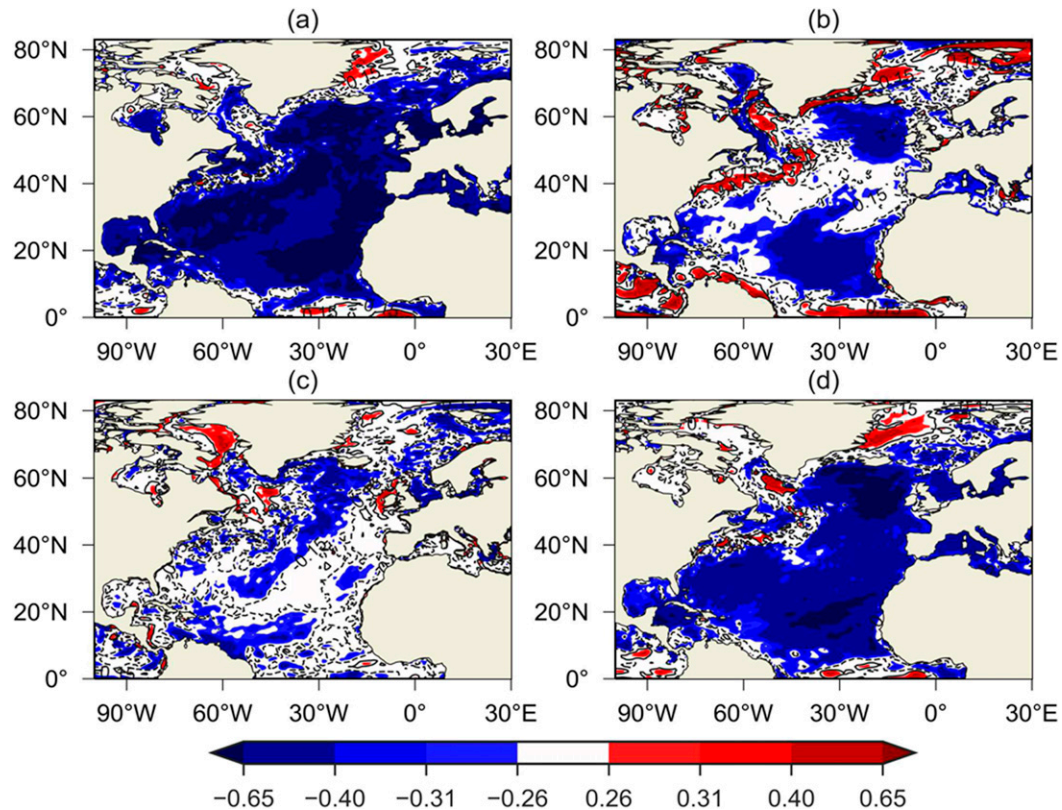
FIG. 4. The correlation between January heat flux anomaly and (a) January tendency of surface temperature anomalies, (b) January surface temperature anomalies, (c) February surface temperature tendency anomalies, and (d) February surface temperature anomalies. Correlations are calculated across the 40 ensembles for each year and then averaged over 35 years. Colors represent the correlation passing statistical significance tests with confidence levels of 90% at ±0.26, 95% at ±0.31 and 99% at ±0.40.

However, along the eastern side of Greenland there is a strong negative correlation up to -0.6 between anomalies in the air–sea heat flux and the same and following month's sea ice fraction (following month correlation map not shown). During winter there is a relatively large fraction of sea ice here (see Fig. 5b) that acts to limit the heat loss from the warmer sea to the colder atmosphere. However, if the extent of sea ice reduces, there is more heat loss from the ocean to the atmosphere due to a greater extent of warmer open surface in contact with the atmosphere (Fig. 5a). The localized positive correlation between anomalies in the surface heat flux and surface temperature (Figs. 4b,d) also suggests that the extent of the sea ice may have a controlling effect on the air–sea heat fluxes, rather than always responding to the air–sea heat fluxes.

5. The effect of the atmospheric jet on the surface ocean

Variations in the jet stream bring different air masses zonally and meridionally over the Atlantic and the air–sea exchange of heat, altering the surface temperature and sea ice distributions. A composite analysis is next provided to help validate the relationships emerging from the model ensemble versus the reanalysis and then a sensitivity analysis is provided for the ensemble data.

a. Composite analysis of how surface ocean properties connect to jet indices

The monthly ensemble data over 35 winters are analyzed in terms of how the jet indices connect to anomalies in the surface properties, based on the difference in January for a composite of 200 months of the highest index minus the same for the lowest index (following the same selection rules as in section 3). These 200 ensemble members for high and low indices are spread over the entire time record from 1980 to 2014, rather than being biased to particular decades.

A composite analysis for the combined anomalies in surface latent and sensible heat fluxes associated with a stronger jet reveals a clear tripole pattern over the North Atlantic (Fig. 6a) with a greater ocean heat loss by $90\,\mathrm{W\,m^{-2}}$ over much of the subpolar region and eastern
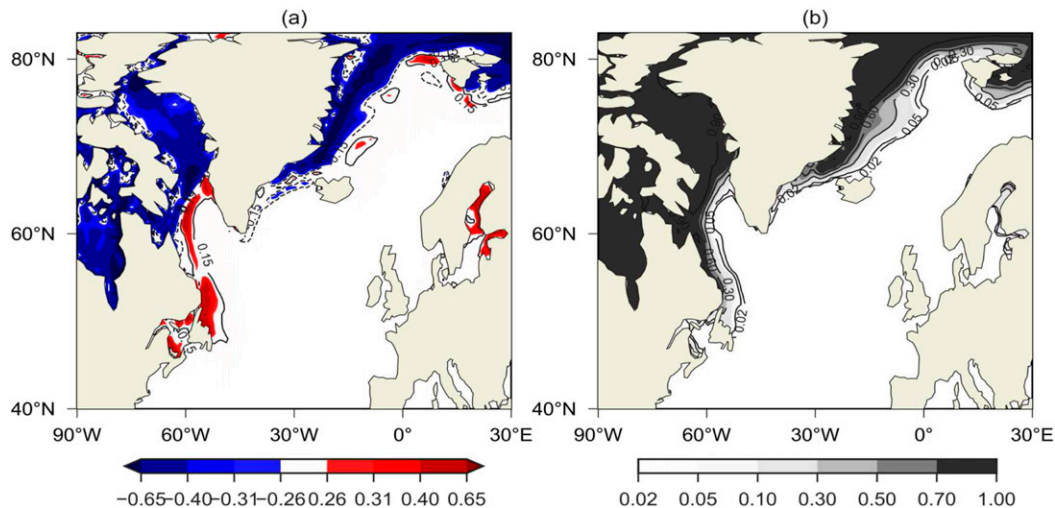
FIG. 5. (a) The correlation between January surface heat flux anomaly and January sea ice fraction anomaly across the 40 ensembles for each year and then averaged over 35 years. Colors represent the correlation passing statistical significance tests as in Fig. 4. (b) January sea ice fraction climatology mean.

side of the tropics, together with an ocean heat gain by $-70\,\mathrm{W\,m^{-2}}$ along the Gulf Stream. Changes in the jet latitude provide a broadly similar tripole pattern, but with more localized loss of heat over the subpolar gyre and a more extensive gain of heat over the subtropics (Fig. 6b).

The corresponding composite analysis for surface temperature reveals that increasing jet speed or latitude is associated with colder surface waters over the Labrador and Irminger Seas with anomalies reaching $-1.0\,^{\circ}\mathrm{C}$, parts of the subpolar gyre and the eastern tropics up to from $-0.5\,^{\circ}$ to $-0.7\,^{\circ}\mathrm{C}$, but warmer surface waters over much of the subtropics are about $0.5\,^{\circ}$–$0.7\,^{\circ}\mathrm{C}$ and the Nordic seas over $1.0\,^{\circ}\mathrm{C}$ (Figs. 6c,d), which we know may due to warm air advection transported there (see Figs. 2e–h). Over most of the domain the sign of the sea surface temperature anomaly is consistent with a greater surface heat loss driving cooling. The more northern jet is particularly associated with a northward extension of the subtropical gyre (Fig. 3c).

There are broadly similar patterns when the composites are evaluated from ERA-Interim reanalysis monthly and daily data during winter from years 1980 to 2014. The daily time-scale fields have very similar tripole patterns to the ensemble monthly fields, albeit with a greater heat loss of $150\,\mathrm{W\,m^{-2}}$ in the subpolar region (Figs. 7e,f). This increased magnitude is simply explained by the increased range of jet speed in the daily data compared to the monthly. This comparison reveals that the ensemble model and reanalysis data exhibit similar relationships between jet stream and surface ocean variability, supporting the use of the ensemble data to investigate causality in this relationship.

There are some detailed differences in the surface heat flux and sea surface temperature anomalies in monthly ensemble and reanalysis fields. First, a stronger jet in the reanalysis is associated with a greater surface heat loss extending over the eastern side of the Atlantic and hence lower sea surface temperatures compared to the model (Figs. 7a,c). This response might reflect the observed association between the jet speed and Atlantic multidecadal variability in surface temperature since NAO variablity is dominated by jet speed strength with time scales greater than 30 years (Woollings et al. 2015; Häkkinen et al. 2011). Second, a more northern jet in the reanalysis is associated with an anomalous gain in ocean heat in the subtropical region and a more extensive downstream increase in surface temperature compared to the model (Figs. 7b,d,f).

The contrasting patterns of heat flux associated with the jet latitude and speed indices may indicate different affects on the ocean subtropical and subpolar gyres, with their climatological boundaries indicated by the climatological Ekman upwelling (black lines in Figs. 6a,b and 7a,b). The variations in jet latitude are seen to be particularly closely related to the gyres: a more northern jet leads to the northern region of upward heat flux anomaly lying entirely within the subpolar gyre and the downward heat flux anomalies closely following the boundary between subtropical and subpolar gyres (Figs. 6b and 7b).

b. The sensitivity of the surface heat flux to the jet indices

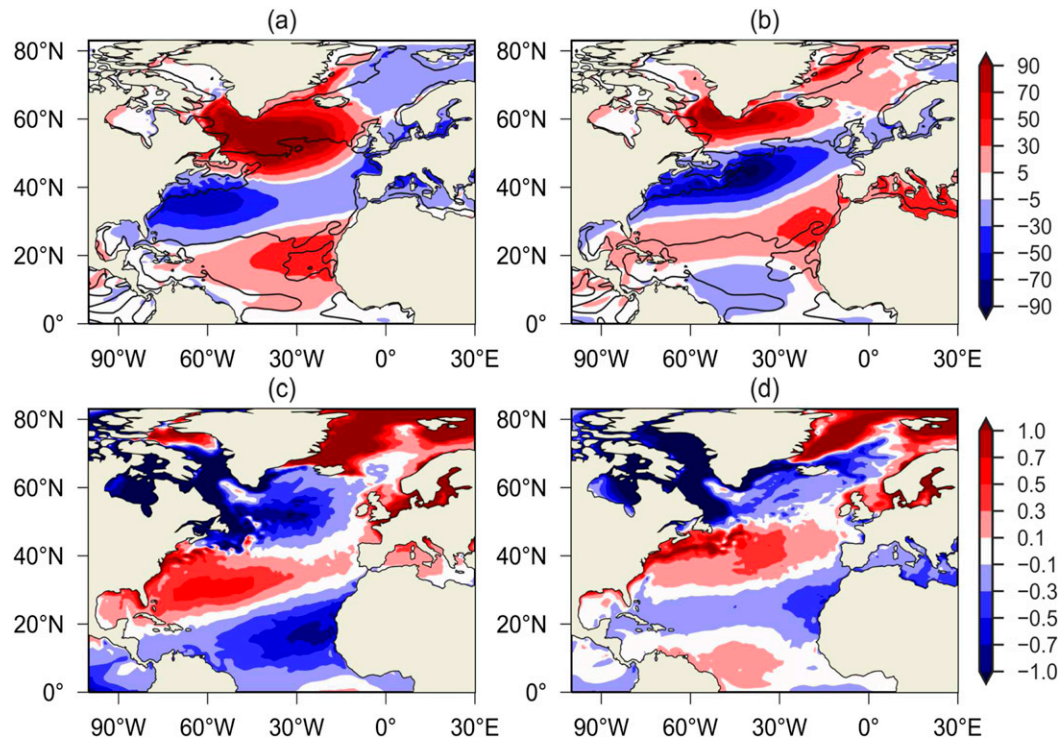To begin the sensitivity analysis, the correlation across the 40 ensemble members initialized at the start of

FIG. 6. Surface heat flux difference (W m^{-2}) using ensemble data across 1980–2014 between a composite of 200 January months of (a) the highest jet speed minus that for the lowest jet speed and (b) the highest jet latitude minus that for the lowest jet latitude (where a positive represents a greater ocean heat loss). Surface temperature difference (°C) between a composite of 200 January months of (c) the highest speed minus that for the lowest jet speed and (d) the highest jet latitude minus that for the lowest jet latitude. The demarcation of the ocean gyres are indicated by the zero lines in the climatological-mean Ekman upwelling velocity in (a) and (b).

November is calculated for each winter month between the precursor jet indices and target heat flux fields over the North Atlantic. The mean correlations of January jet speed and latitude with January heat flux show robust tripole patterns over the entire North Atlantic (Fig. 8), which implies the North Atlantic surface sensible and latent heat flux are strongly sensitive to the jet speed and latitude shifts in wintertime.

The correlation signals are similar to the composite anomaly patterns (Figs. 6a,b and 7a,b,e,f). The positive correlation centers are located over much of the subpolar region and the tropics. The maximum positive correlation reaches values over 0.6 around the subpolar region, so that strong and northward shifted jets both cause greater heat loss from the ocean to the atmosphere. However, an opposite correlation is seen over the subtropics, which suggests that strong and northward shifted jets reduce heat loss from the ocean to the atmosphere in this region. The correlation patterns for the ensemble show subtle differences, with jet speed affecting heat fluxes more strongly in the tropical and subpolar regions, but jet latitude affecting heat fluxes by

shifting their pattern farther north in both tropical and subtropical regions (Figs. 8a,b).

c. The sensitivity of sea surface temperature to the jet indices

In a similar manner, the ensemble sensitivity analysis for surface temperature and jet speed again reveals the characteristic tripole pattern (Figs. 9a–d). Their correlation is relatively weak when comparing January jet speed and January surface temperature (Fig. 9a), but strengthens when comparing January jet speed and February temperature with large regions exceeding the 99% confidence level (Fig. 9b), and this signal persists into March and only weakens by April (Figs. 9c,d). Hence, a strong jet speed causes more heat flux to be released from the ocean to the atmosphere, driving a cooling of surface temperature that persists for at least four months.

The ensemble sensitivity for surface temperature and jet latitude only reveals a weak connection for the same month of January in regions around the north of Iceland and the northwest Labrador Sea (Figs. 9e–h). The characteristic tripole pattern only appears in the following
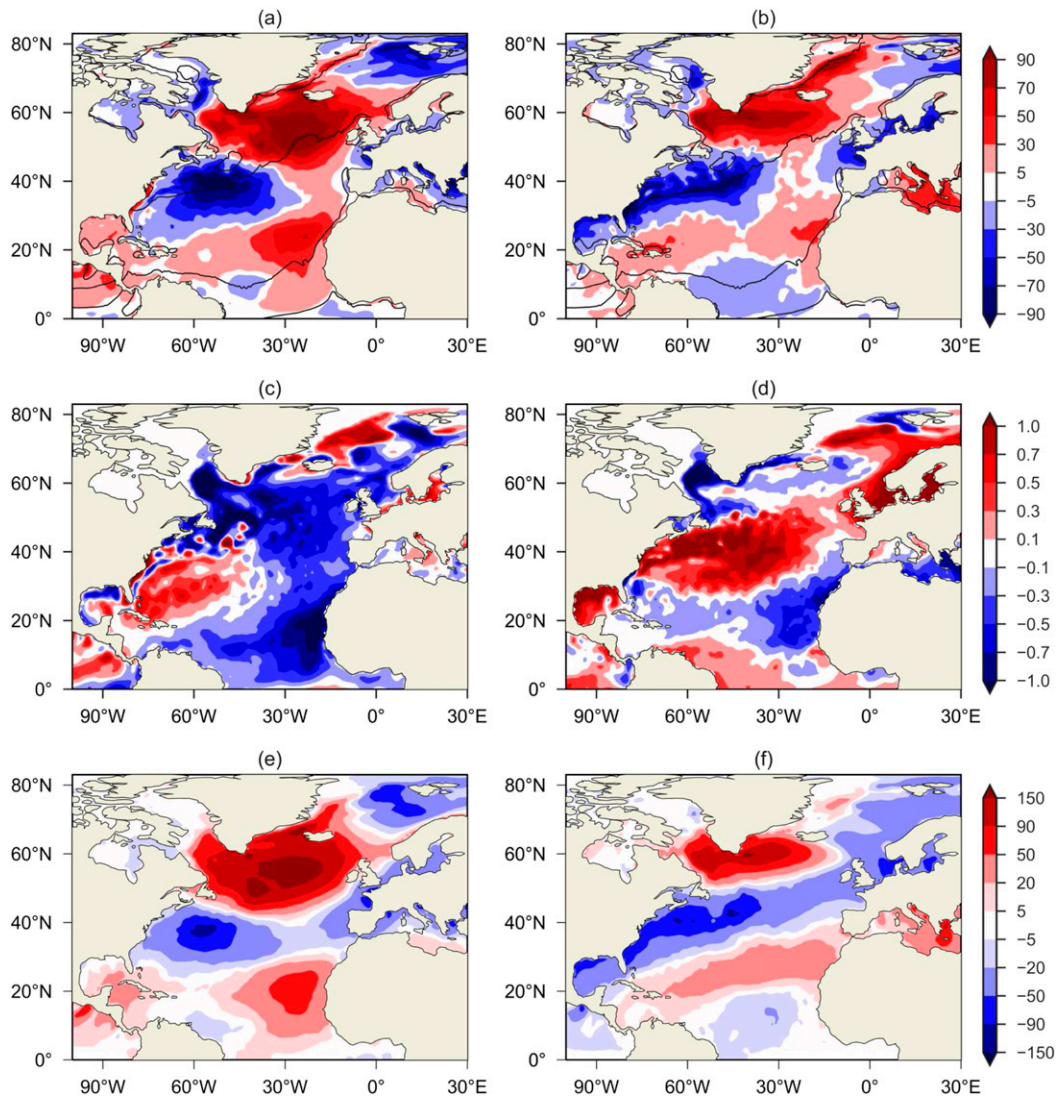
FIG. 7. Surface heat flux difference (W m^{-2}) using ERA-Interim reanalysis monthly data across 1980–2014 between a composite of seven January months of (a) the highest jet speed minus that for the lowest jet speed and (b) the highest jet latitude minus that for the lowest jet latitude (where positive represents a greater ocean heat loss). February surface temperature differences (°C) between a composite of January months for (c) the highest jet speed minus that for the lowest jet speed and (d) the highest jet latitude minus that for the lowest jet latitude. Surface heat flux difference (W m^{-2}) using ERA-Interim reanalysis daily data across 1980–2014 between a composite of 200 January days of (e) the highest jet speed minus that for the lowest jet speed and (f) the highest jet latitude minus that for the lowest jet latitude (where positive represents a greater ocean heat loss). The demarcation of the ocean gyres are indicated by the zero lines in the climatological-mean Ekman upwelling velocity in (a) and (b).

months, peaking again at a 1-month lag in February (Fig. 9f), but then the signal is relatively short lived and decays from March to April (Figs. 9g,h).

d. Composite analysis and sensitivity of sea ice to the jet indices

The sensitivity of the sea ice extent is now considered in terms of the jet indices. Changes in sea ice coverage, motion and thickness have been previously associated

with different atmospheric states, as defined by the NAO and Arctic Oscillation (AO) (Alexander et al. 2004; Pedersen et al. 2016; Hilmer and Jung 2000).

The relationship between the jet indices and surface temperature around the boundaries of the subpolar gyre, particularly for the Greenland and Labrador Seas, may be associated with direct effects of the air–sea heat fluxes and changes in sea ice extent. The surface temperature is the same as sea surface temperature when
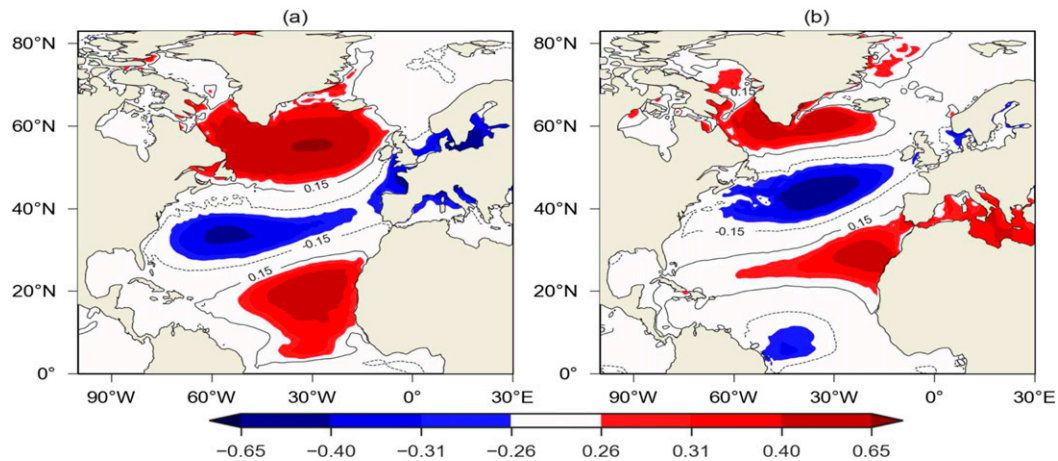
FIG. 8. The correlation between January surface heat flux and (a) January jet speed and (b) January jet latitude across the 40 ensembles for each year and then averaged over 35 years. Colors represent the correlation passing statistical significance tests as in Fig. 4.

there is open water, but is elsewhere taken as the surface temperature of the land or ice. Using both ensemble and reanalysis data, the composite analysis for sea ice fraction reveals that a stronger or more northern jet is associated with reduced sea ice cover north of Iceland and around the Nordic seas (Fig. 10). This signal is consistent with the jet stream extending to higher latitudes. In addition, a stronger jet is associated with greater heat loss over the Labrador Sea acting to cool surface waters and enhance the fraction of sea ice by 30% (Figs. 10a,c). In contrast, a more northern or stronger jet typically leads to a 20%–30% reduction in sea ice fraction over the east Greenland Sea (Fig. 10) due to warm air advection transported there (Figs. 2e–h).

The ensemble sensitivity of the sea ice fraction reveals that there is a stronger effect of the jet speed and latitude when evaluated over the whole winter period, December–February (DJF) (Fig. 11), rather than for individual months. The correlation between winter-mean jet speed and February sea ice fraction across 40 ensembles reveals a dipole pattern with positive signals along the Labrador Sea boundary and negative signals along the east Greenland Sea, which implies sea ice fraction is increasing over the Labrador Sea and decreasing over the east Greenland Sea during strong jet speed periods (Fig. 11a). A similar correlation dipole pattern is shown between winter jet latitude and the February sea ice fraction (Fig. 11b). There is also a similar correlation pattern between the sea ice fraction and NAO based upon the ensemble sensitivity analysis (not shown).

A stronger or northward-shifted jet increases cold air advection from west Greenland and Baffin Bay or the continent (Fig. 2), which may affect the sea ice fraction in the Labrador Sea in two different ways: (i) a thermal

effect of cold air causing more surface heat loss, decreasing the water surface temperature and growing more sea ice, and (ii) a mechanical effect of more sea ice blown to the Labrador sea from upstream–west Greenland and Baffin Bay, in particular with a strong jet having more effect than jet latitude over Baffin Bay where we can see there is a negative correlation implying a reduction of sea ice fraction there (Fig. 11a).

The response over the east Greenland Sea may involve different variants on these thermal and mechanical responses: (i) a stronger or northward-shifted jet enhances the warm air transported there (Fig. 2) reducing ice cover and leading to an increase in surface temperature as the open ocean replaces sea ice coverage; and (ii) a strong northerly wind along the east Greenland coast blows surface ice away from the Fram Strait and may also be linked to AO-related wind changes over the Arctic basin that encourage a thinning of the ice (Rigor et al. 2002). There is a noticeable difference over the west of Iceland where sea ice increases to the west of Iceland under a northern jet (Fig. 11b) likely due to an extension of the Labrador cold air advection around the southern tip of Greenland (Fig. 2c).

6. Quantifying the sensitivity of the ocean surface variables to the jet indices

a. Normalization of the sensitivity analyses

The ensemble sensitivity analysis is now normalized to quantify changes in surface heat flux, surface temperature, and sea ice fraction resulting from changes in jet speed and latitude. The normalization expresses units of change in outcome J per standard deviation of predictor x across the ensemble using Eq. (1). The normalization
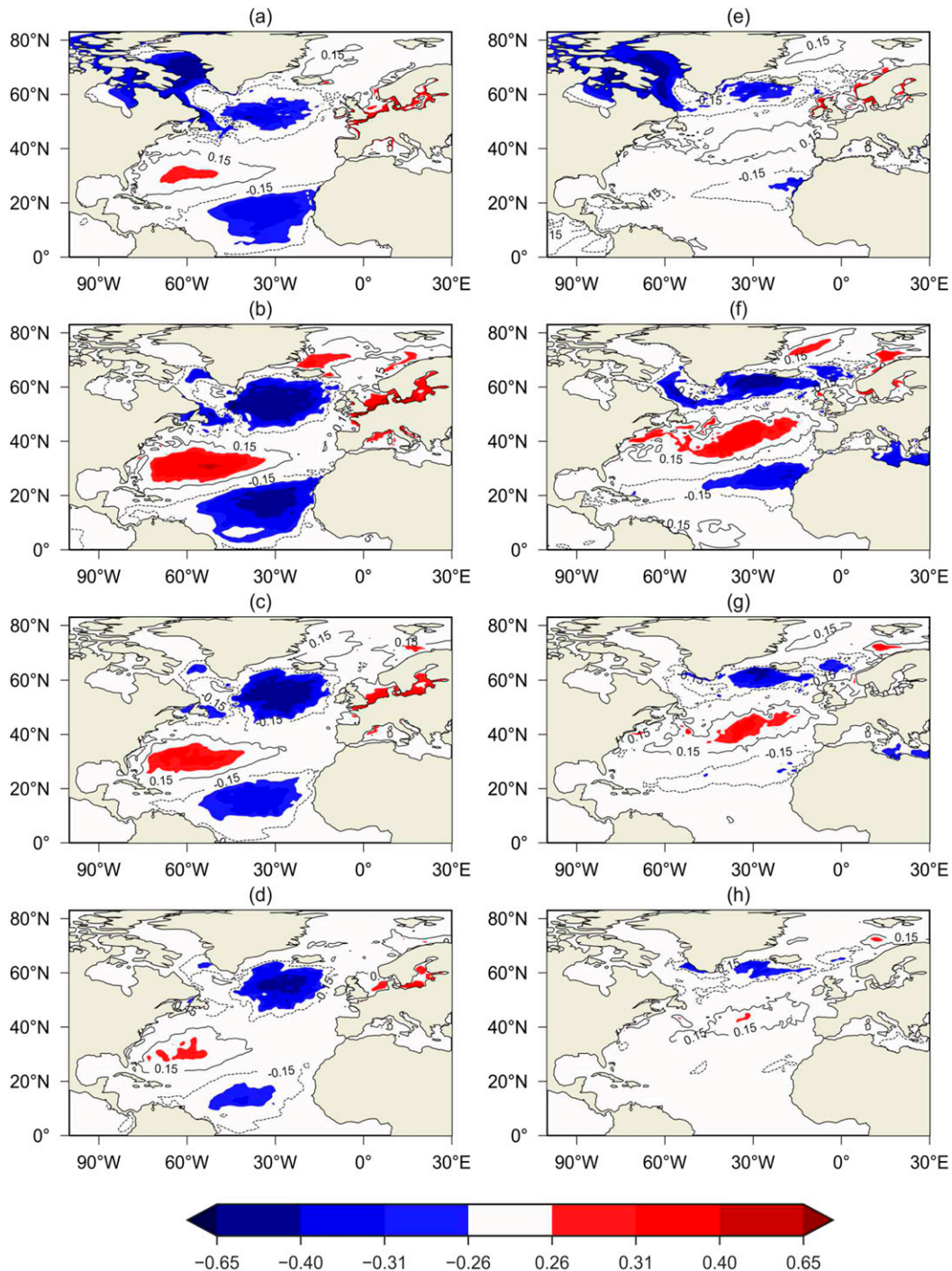
FIG. 9. The correlation between January jet speed and (a) January surface temperature, (b) February surface temperature, (c) March surface temperature, and (d) April surface temperature, and the correlation between January jet latitude and (e) January surface temperature, (f) February surface temperature, (g) March surface temperature, and (h) April surface temperature. Correlations are taken across the 40 ensembles for each year and then averaged over 35 years. Colors represent the correlation passing statistical significance tests as in Fig. 4.
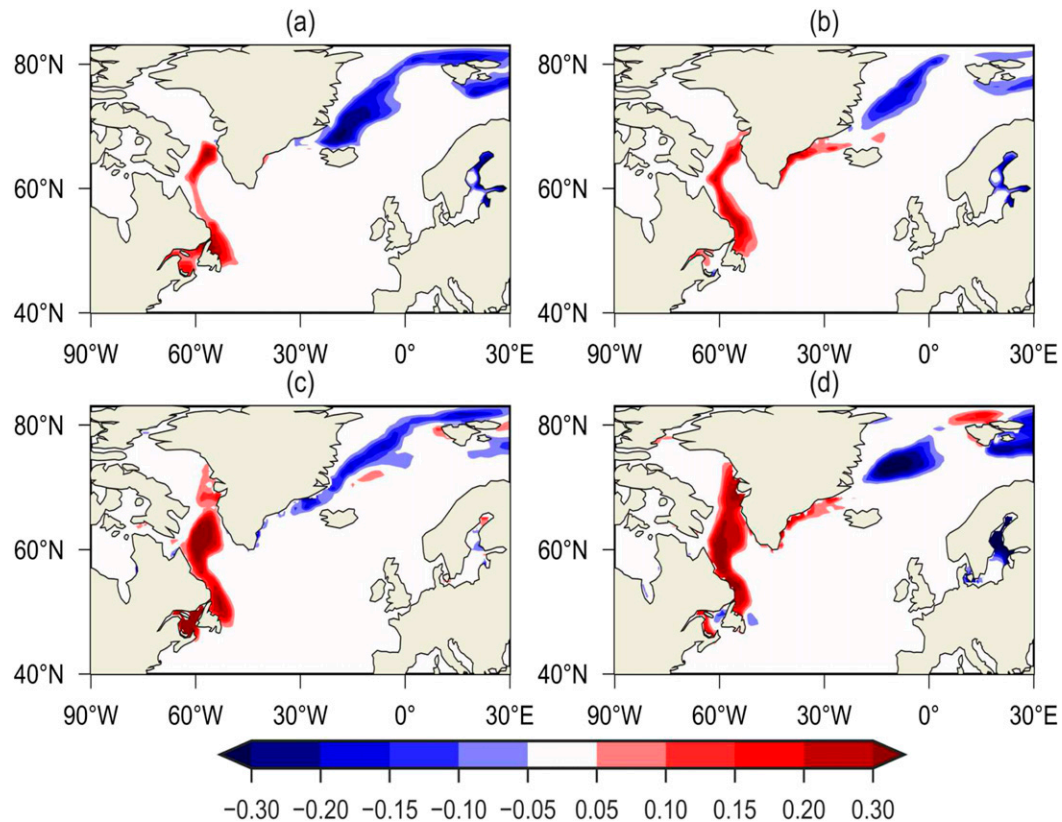
FIG. 10. February sea ice fraction difference between a composite of 200 January months from ensemble data of (a) the highest jet speed minus that for the lowest jet speed and (b) the highest jet latitude minus that for the lowest jet latitude. February sea ice fraction difference between a composite of seven January months from reanalysis data of (c) the highest jet speed minus that for the lowest jet speed and (d) the highest jet latitude minus that for the lowest jet latitude.

reveals that a standard deviation in January jet speed is associated with a change in the January surface heat flux by up to 35–40 W m^{-2} over the subpolar region (Fig. 12a) and a change in the February surface temperature by up to 0.3°C across large regions of the open sea (Fig. 12c). A standard deviation change in jet latitude leads to a similar magnitude response in the heat flux anomalies, although of a reduced extent (Fig. 12b), and the ocean temperature response is also weaker apart from a band of strong positive anomalies of over 0.5°C along the Gulf Stream (Fig. 12d).

A standard deviation in winter-mean jet speed or latitude leads to changes in February sea ice fraction of around 10%–15% (Figs. 12e,f).

b. The proportion of surface ocean variability controlled by the jet indices

The extent that the atmospheric jet affects the variability of the surface ocean is assessed by performing a linear regression between both the surface heat flux and sea surface temperature with the indices for jet speed and latitude across 40 ensembles each year, then a climatological mean is taken over 35 years. The regression estimate of January surface heat flux based on January jet speed suggests that 40%–50% of the total variance in heat flux is explained by the variance in jet speed over the subpolar region (Fig. 13a); the shaded values in Fig. 13 are expressed in terms of R^2, which measures the ratio of the explained variance to the total variance.

Meanwhile, the regression estimate of February surface temperature based on January jet speed suggests that 35% of the surface temperature variation in February is explained by the January jet speed (Fig. 13c). The regression estimates of surface heat flux variation and surface temperature explained by changes in jet latitude are weaker than those based on jet speed (Figs. 13b,d). This response implies that nearly half of the heat flux variance and a third of the temperature variance is explained by the jet indices with jet speed showing a stronger relationship than jet latitude.

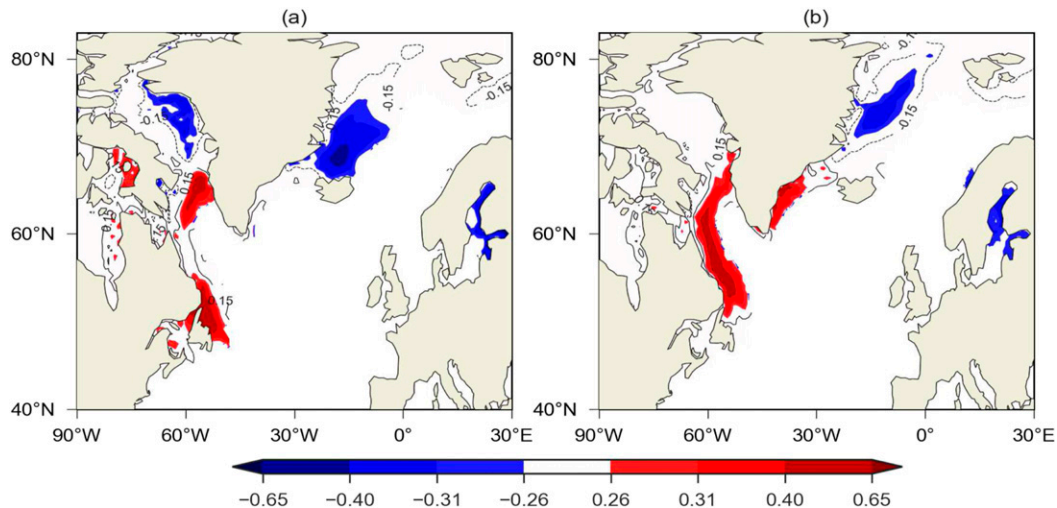The regression estimate of February sea ice fraction variance based on winter jet indices explains about

FIG. 11. The correlation between (a) winter DJF mean jet speed and February sea ice fraction and (b) winter DJF mean jet latitude and February sea ice fraction. Correlations are taken across the 40 ensembles for each year and then averaged over 35 years. Colors represent the correlation passing statistical significance tests as in Fig. 4.

20%–35% of the variance in the Labrador Sea, whereas the February sea ice fraction variance is explained by the winter jet indices of about 20% and a smaller region reaching 35% in the east Greenland Sea (Figs. 13e,f).

7. Discussion and conclusions

The role of the atmosphere in driving the surface ocean in the North Atlantic is explored here on monthly and seasonal time scales. The dominant atmospheric phenomenon in the midlatitudes is the eddy-driven jet stream, affecting the formation and passage of synoptic-scale weather systems, and the emergence of weather regimes and blocking patterns (Cassou et al. 2004, 2011; Barrier et al. 2014). The sensitivity of the air–sea heat flux, sea surface temperature, and sea ice extent are explored using a coupled atmosphere–ocean model dataset made up of 40 ensemble members initialized each November and repeated over 35 years.

The atmospheric jet strongly affects the wintertime pattern of air–sea latent and sensible heat flux anomalies, altering sea surface temperature anomalies, and the winter sea ice distribution. For example, a standard deviation change in the jet speed or latitude typically results in surface heat flux anomalies of the order of 20–30 W m^{-2} over much of the North Atlantic together with surface temperatures anomalies of typically 0.2°–0.3°C in the open ocean, and changes in sea ice fraction of 15% in the Labrador and Greenland Sea regions.

The effect of the atmospheric jet on the surface heat flux anomalies leads to a corresponding imprint on surface temperature anomalies. Over most of the surface ocean, enhanced surface heat loss drives the expected surface cooling (Cayan 1992; Gulev et al. 2013), although departures in this local heat balance occur over the Gulf Stream associated with its advection of heat (Roberts et al. 2017).

The patterns of surface ocean response are broadly consistent with the relationship between the empirical mode of the North Atlantic Oscillation and the surface ocean (Marshall et al. 2001; Visbeck et al. 2003). However, the speed and latitude of the jet are two physically distinct types of atmospheric variability. While both types of variability project onto the NAO and are related to tripole patterns in heat flux and sea surface temperature, the jet indices have subtly different effects on the surface ocean. Both jet strength and latitude lead to different thermodynamical and dynamical effects. For example, a thermodynamical effect of the jet is in altering the surface circulation and the advection of warm and cold air anomalies (as in Fig. 2), which are crucial for air–sea heat exchange. A dynamical effect of the jet is by a strong jet enhancing the magnitude of the wind-induced Ekman horizontal and vertical transport (as in Fig. 3), and the jet latitude altering their pattern and so shifting the position of the ocean gyre boundaries. On time scale of several months, the jet speed is shown to have a stronger affect on the ocean surface anomalies than jet latitude, with stronger heat flux anomalies leading to larger surface temperature anomalies that persist for longer.

The atmospheric jet alters the sea ice distribution over winter in two different ways. In regions of extensive ice cover, such as along the eastern side of Greenland, a stronger jet is associated with a reduction in sea ice connected with an emergence of warmer surface waters,
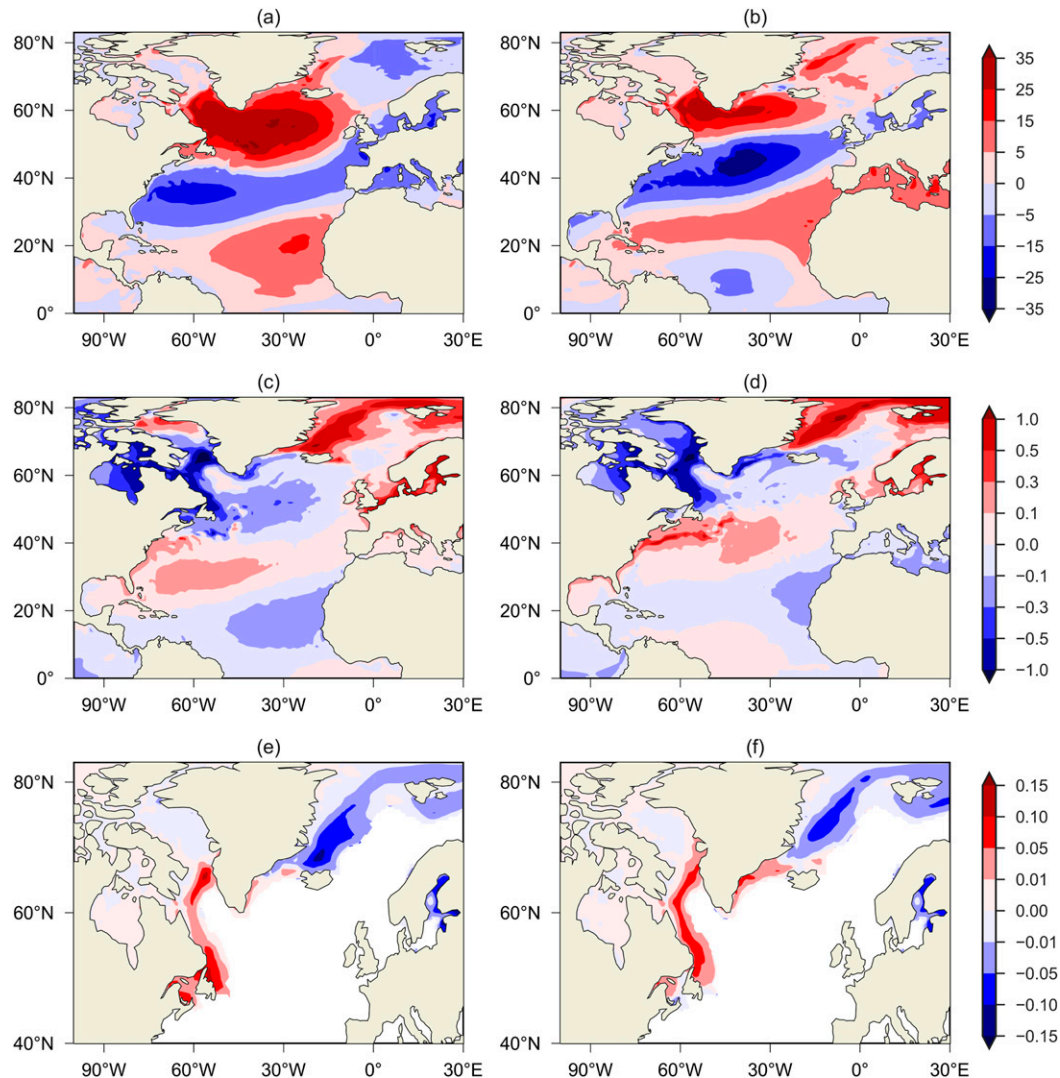
FIG. 12. Normalized dependence of (a) January surface heat flux (W m^{-2}) per standard deviation of January jet speed, (b) January surface heat flux (W m^{-2}) per standard deviation of January jet latitude, (c) February surface temperature (°C) per standard deviation of January jet speed, (d) February surface temperature (°C) per standard deviation of January jet latitude, (e) February sea ice fraction per standard deviation of DJF mean jet speed, and (f) February sea ice fraction per standard deviation of DJF mean jet latitude. Normalizations are made across the 40 ensembles for each year and then averaged over 35 years.

which in turn drives a greater surface heat loss. In contrast, in regions of less ice extent, such as in the Labrador Sea, a stronger jet is associated with a greater surface cooling, which leads to more sea ice cover.

Our study assesses the effect of the atmospheric jet on the surface ocean using monthly ensemble data, which omits the effect of submonthly synoptic weather variability that may be important Ogawa and Spengler (2019). To test this simplification, we compare how the jet indices connect to surface heat flux using daily reanalysis data versus monthly ensemble and reanalysis data and find that their relationships are broadly similar.

While synoptic meridional winds generate large heat flux anomalies on a daily time scale, the alternating effects of southerly and northerly winds to a large extent cancel out in the monthly average, as indeed suggested by Ogawa and Spengler (2019). Hence, monthly time-scale variability in the eddy-driven jet alone can account for a significant fraction of the North Atlantic sea surface temperature changes that develop during the winter. The remaining sea surface temperature variance will likely be influenced by other large-scale atmospheric patterns, as well as synoptic variability and ocean internal dynamics.
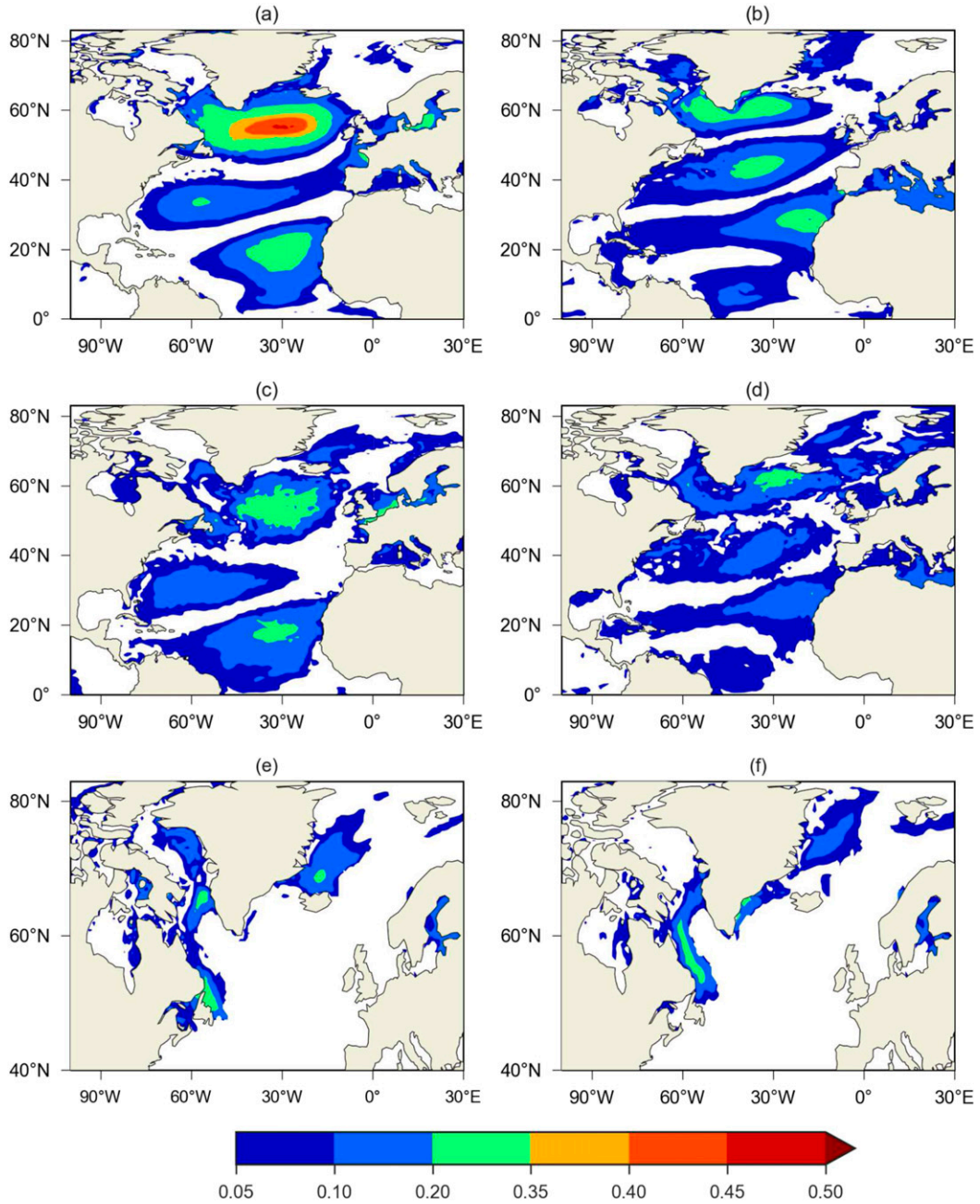
FIG. 13. The proportion of the variance of the January surface heat flux that is explained by a linear regression between surface heat flux and (a) January jet speed and (b) January jet latitude; and the proportion of the variance of the February surface temperature explained by a linear regression between surface temperature and (c) January jet speed and (d) January jet latitude; and the proportion of the variance of the February sea ice fraction explained by a linear regression between sea ice fraction and (e) DJF jet speed and (f) DJF jet latitude. Linear regressions are made across 40 ensembles for each year and then averaged over 35 years.

Ocean dynamics is important in generating ocean internal variability, which may possibly also modify atmospheric variability. However, our sensitivity analysis of the spread in ensembles for each year reveals that ocean surface temperature is not correlated to subsequent

monthly estimates of the jet speed strength and latitude shifts, so we have not found any statistically significant signals of the ocean variability driving subsequent changes in the atmospheric jet stream when averaged over the 35 years of model data. There may be individual winters

where a preceding winter has some effect on the subsequent winter, such as related to re-emergence of subsurface temperature anomalies, but these signals are not statistically significant when averaged over the full record.

In comparison, there are studies arguing that the jet stream is influenced by ocean surface temperature on longer, interannual time scales, where the NAO is found to be sensitive to imposed surface temperature in an atmosphere-only model (Rodwell et al. 1999) and where there may be a positive feedback between the atmospheric circulation and surface temperature (Czaja and Frankignoul 2002). Recently, Baker et al. (2019) used an atmosphere-only linear statistical–dynamical model to identify that indices of jet latitude and jet speed are sensitive to surface temperature, finding that each of these two indices depends upon subtly different patterns of North Atlantic surface temperature. Comparing their sensitivity maps to our results shows agreement between several of the anomalies, so that the temperature anomalies due to jet variability are similar to the patterns of surface temperature that could force the jet.

In summary, variability in the atmospheric eddy-driven jet strongly affects seasonal variability in the surface ocean over the North Atlantic, controlling nearly half of the variance in air–sea heat fluxes and over a third of the subsequent surface temperature variance. There is also a strong imprint on sea ice fraction, a stronger jet acting to enhance the sea ice fraction in relatively ice-depleted regions, but to reduce the sea ice fraction in relatively ice-extensive regions. There are subtle differences in how indices of jet speed and location affect the surface ocean with the effect of jet speed being generally more pronounced than that of jet latitude, although the effect of jet latitude is important in defining the location of the regional response.

REFERENCES

Alexander, M. A., U. S. Bhatt, J. E. Walsh, M. S. Timlin, J. S. Miller, and J. D. Scott, 2004: The atmospheric response to realistic Arctic sea ice anomalies in an AGCM during winter. *J. Climate*, **17**, 890–905, https://doi.org/10.1175/1520-0442(2004)017<0890:TARTRA>2.0.CO;2.

Baker, H. S., T. Woollings, and C. Mbengue, 2017: Eddy-driven jet sensitivity to diabatic heating in an idealized GCM. *J. Climate*, **30**, 6413–6431, https://doi.org/10.1175/JCLI-D-16-0864.1.

——, ——, C. E. Forest, and M. R. Allen, 2019: The linear sensitivity of the North Atlantic Oscillation and eddy-driven jet to

SSTs. *J. Climate*, **32**, 6491–6511, https://doi.org/10.1175/JCLI-D-19-0038.1.

Barrier, N., C. Cassou, J. Deshayes, and A.-M. Treguier, 2014: Response of North Atlantic Ocean circulation to atmospheric weather regimes. *J. Phys. Oceanogr.*, **44**, 179–201, https://doi.org/10.1175/JPO-D-12-0217.1.

Bjerknes, J., 1964: Atlantic air-sea interaction. *Advances in Geophysics*, H. E. Landsberg and J. Van Mieghem, Eds., Vol. 10, Elsevier, 1–82, https://doi.org/10.1016/S0065-2687(08)60005-9.

Bowler, N. E., A. Arribas, S. E. Beare, K. R. Mylne, and G. J. Shutts, 2009: The local ETKF and SKEB: Upgrades to the MOGREPS short-range ensemble prediction system. *Quart. J. Roy. Meteor. Soc.*, **135**, 767–776, https://doi.org/10.1002/qj.394.

Bracegirdle, T. J., H. Lu, R. Eade, and T. Woollings, 2018: Do CMIP5 models reproduce observed low-frequency North Atlantic jet variability? *Geophys. Res. Lett.*, **45**, 7204–7212, https://doi.org/10.1029/2018GL078965.

Cassou, C., L. Terray, J. W. Hurrell, and C. Deser, 2004: North Atlantic winter climate regimes: Spatial asymmetry, stationarity with time, and oceanic forcing. *J. Climate*, **17**, 1055–1068, https://doi.org/10.1175/1520-0442(2004)017<1055:NAWCRS>2.0.CO;2.

——, M. Minvielle, L. Terray, and C. Périgaud, 2011: A statistical–dynamical scheme for reconstructing ocean forcing in the Atlantic. Part I: Weather regimes as predictors for ocean surface variables. *Climate Dyn.*, **36**, 19–39, https://doi.org/10.1007/s00382-010-0781-7.

Cayan, D. R., 1992: Latent and sensible heat flux anomalies over the northern oceans: Driving the sea surface temperature. *J. Phys. Oceanogr.*, **22**, 859–881, https://doi.org/10.1175/1520-0485(1992)022<0859:LASHFA>2.0.CO;2.

Czaja, A., 2009: Atmospheric control on the thermohaline circulation. *J. Phys. Oceanogr.*, **39**, 234–247, https://doi.org/10.1175/2008JPO3897.1.

——, and C. Frankignoul, 2002: Observed impact of Atlantic SST anomalies on the North Atlantic Oscillation. *J. Climate*, **15**, 606–623, https://doi.org/10.1175/1520-0442(2002)015<0606:OIOASA>2.0.CO;2.

Dunstone, N., D. Smith, A. Scaife, L. Hermanson, R. Eade, N. Robinson, M. Andrews, and J. Knight, 2016: Skilful predictions of the winter North Atlantic Oscillation one year ahead. *Nat. Geosci.*, **9**, 809–814, https://doi.org/10.1038/ngeo2824.

Eden, C., and J. Willebrand, 2001: Mechanism of interannual to decadal variability of the North Atlantic circulation. *J. Climate*, **14**, 2266–2280, https://doi.org/10.1175/1520-0442(2001)014<2266:MOITDV>2.0.CO;2.

Grist, J. P., and Coauthors, 2010: The roles of surface heat flux and ocean heat transport convergence in determining Atlantic Ocean temperature variability. *Ocean Dyn.*, **60**, 771–790, https://doi.org/10.1007/s10236-010-0292-4.

Gulev, S. K., M. Latif, N. Keenlyside, W. Park, and K. P. Koltermann, 2013: North Atlantic Ocean control on surface heat flux on multidecadal timescales. *Nature*, **499**, 464–467, https://doi.org/10.1038/nature12268.

Häkkinen, S., P. B. Rhines, and D. L. Worthen, 2011: Atmospheric blocking and Atlantic multidecadal ocean variability. *Science*, **334**, 655–659, https://doi.org/10.1126/science.1205683.

Hilmer, M., and T. Jung, 2000: Evidence for a recent change in the link between the North Atlantic Oscillation and Arctic sea ice export. *Geophys. Res. Lett.*, **27**, 989–992, https://doi.org/10.1029/1999GL010944.

Hoskins, B. J., I. N. James, and G. H. White, 1983: The shape, propagation and mean-flow interaction of large-scale weather systems. *J. Atmos. Sci.*, **40**, 1595–1612, https://doi.org/10.1175/1520-0469(1983)040<1595:TSPAMF>2.0.CO;2.

Hurrell, J. W., and C. Deser, 2010: North Atlantic climate variability: The role of the North Atlantic Oscillation. *J. Mar. Syst.*, **79**, 231–244, https://doi.org/10.1016/j.jmarsys.2009.11.002.

Isemer, H.-J., and L. Hasse, 1987: *Air-Sea Interactions*. Vol. 2, *The Bunker Climate Atlas of the North Atlantic Ocean*, Spring-Verlag, 252 pp.

Johnson, N. C., S. B. Feldstein, and B. Tremblay, 2008: The continuum of Northern Hemisphere teleconnection patterns and a description of the NAO shift with the use of self-organizing maps. *J. Climate*, **21**, 6354–6371, https://doi.org/10.1175/2008JCLI2380.1.

Kim, W. M., S. Yeager, P. Chang, and G. Danabasoglu, 2018: Low-frequency North Atlantic climate variability in the Community Earth System Model large ensemble. *J. Climate*, **31**, 787–813, https://doi.org/10.1175/JCLI-D-17-0193.1.

Knight, J. R., C. K. Folland, and A. A. Scaife, 2006: Climate impacts of the Atlantic Multidecadal Oscillation. *Geophys. Res. Lett.*, **33**, L17706, https://doi.org/10.1029/2006GL026242.

Kolstad, E. W., T. J. Bracegirdle, and I. A. Seierstad, 2009: Marine cold-air outbreaks in the North Atlantic: Temporal distribution and associations with large-scale atmospheric circulation. *Climate Dyn.*, **33**, 187–197, https://doi.org/10.1007/s00382-008-0431-5.

Kravtsov, S., 2017: Pronounced differences between observed and CMIP5-simulated multidecadal climate variability in the twentieth century. *Geophys. Res. Lett.*, **44**, 5749–5757, https://doi.org/10.1002/2017GL074016.

Lozier, M. S., S. Leadbetter, R. G. Williams, V. Roussenov, M. S. C. Reed, and N. J. Moore, 2008: The spatial pattern and mechanisms of heat content change in the North Atlantic. *Science*, **319**, 800–803, https://doi.org/10.1126/science.1146436.

——, V. Roussenov, M. S. C. Reed, and R. G. Williams, 2010: Opposing decadal changes for the North Atlantic meridional overturning circulation. *Nat. Geosci.*, **3**, 728–734, https://doi.org/10.1038/ngeo947.

Madonna, E., C. Li, C. M. Grams, and T. Woollings, 2017: The link between eddy-driven jet variability and weather regimes in the North Atlantic-European sector. *Quart. J. Roy. Meteor. Soc.*, **143**, 2960–2972, https://doi.org/10.1002/qj.3155.

Marshall, J., and Coauthors, 2001a: North Atlantic climate variability: Phenomena, impacts and mechanisms. *Int. J. Climatol.*, **21**, 1863–1898, https://doi.org/10.1002/joc.693.

——, H. Johnson, and J. Goodman, 2001b: A study of the interaction of the North Atlantic Oscillation with ocean circulation. *J. Climate*, **14**, 1399–1421, https://doi.org/10.1175/1520-0442(2001)014<1399:ASOTIO>2.0.CO;2.

Ogawa, F., and T. Spengler, 2019: Prevailing surface wind direction during air–sea heat exchange. *J. Climate*, **32**, 5601–5617, https://doi.org/10.1175/JCLI-D-18-0752.1.

O'Reilly, C. H., S. Minobe, and A. Kuwano-Yoshida, 2016: The influence of the Gulf Stream on wintertime European blocking. *Climate Dyn.*, **47**, 1545–1567, https://doi.org/10.1007/s00382-015-2919-0.

Papritz, L., and T. Spengler, 2017: A Lagrangian climatology of wintertime cold air outbreaks in the Irminger and Nordic Seas and their role in shaping air–sea heat fluxes. *J. Climate*, **30**, 2717–2737, https://doi.org/10.1175/JCLI-D-16-0605.1.

Parfitt, R., and H. Seo, 2018: A new framework for near-surface wind convergence over the Kuroshio Extension and Gulf Stream in wintertime: The role of atmospheric fronts. *Geophys. Res. Lett.*, **45**, 9909–9918, https://doi.org/10.1029/2018GL080135.

Pedersen, R. A., I. Cvijanovic, P. L. Langen, and B. M. Vinther, 2016: The impact of regional Arctic sea ice loss on atmospheric circulation and the NAO. *J. Climate*, **29**, 889–902, https://doi.org/10.1175/JCLI-D-15-0315.1.

Rigor, I. G., J. M. Wallace, and R. L. Colony, 2002: Response of sea ice to the Arctic Oscillation. *J. Climate*, **15**, 2648–2663, https://doi.org/10.1175/1520-0442(2002)015<2648:ROSITT>2.0.CO;2.

Roberts, C. D., M. D. Palmer, R. P. Allan, D. G. Desbruyeres, P. Hyder, C. Liu, and D. Smith, 2017: Surface flux and ocean heat transport convergence contributions to seasonal and interannual variations of ocean heat content. *J. Geophys. Res. Oceans*, **122**, 726–744, https://doi.org/10.1002/2016JC012278.

Robson, J., R. Sutton, K. Lohmann, D. Smith, and M. D. Palmer, 2012: Causes of the rapid warming of the North Atlantic Ocean in the mid-1990s. *J. Climate*, **25**, 4116–4134, https://doi.org/10.1175/JCLI-D-11-00443.1.

Rodwell, M. J., D. P. Rowell, and C. K. Folland, 1999: Oceanic forcing of the wintertime North Atlantic Oscillation and European climate. *Nature*, **398**, 320–323, https://doi.org/10.1038/18648.

Simpson, I. R., C. Deser, K. A. McKinnon, and E. A. Barnes, 2018: Modeled and observed multidecadal variability in the North Atlantic jet stream and its connection to sea surface temperatures. *J. Climate*, **31**, 8313–8338, https://doi.org/10.1175/JCLI-D-18-0168.1.

Smith, D. M., and J. M. Murphy, 2007: An objective ocean temperature and salinity analysis using covariances from a global climate model. *J. Geophys. Res.*, **112**, C02022, https://doi.org/10.1029/2005JC003172.

——, S. Cusack, A. W. Colman, C. K. Folland, G. R. Harris, and J. M. Murphy, 2007: Improved surface temperature prediction for the coming decade from a global climate model. *Science*, **317**, 796–799, https://doi.org/10.1126/science.1139540.

Sutton, R. T., and B. Dong, 2012: Atlantic Ocean influence on a shift in European climate in the 1990s. *Nat. Geosci.*, **5**, 788–792, https://doi.org/10.1038/ngeo1595.

Thompson, D. W., S. Lee, and M. P. Baldwin, 2003: *Atmospheric Processes Governing the Northern Hemisphere Annular Mode/North Atlantic Oscillation. Geophys. Monogr.*, Vol. 134, Amer. Geophys. Union, 81–112.

Torn, R. D., J. S. Whitaker, P. Pegion, T. M. Hamill, and G. J. Hakim, 2015: Diagnosis of the source of GFS medium-range track errors in Hurricane Sandy (2012). *Mon. Wea. Rev.*, **143**, 132–152, https://doi.org/10.1175/MWR-D-14-00086.1.

Vannière, B., A. Czaja, H. Dacre, and T. Woollings, 2017: A "cold path" for the Gulf Stream–troposphere connection. *J. Climate*, **30**, 1363–1379, https://doi.org/10.1175/JCLI-D-15-0749.1.

Visbeck, M., E. P. Chassignet, R. G. Curry, T. L. Delworth, R. R. Dickson, and G. Krahmann, 2003: The ocean's response to North Atlantic Oscillation variability. *The North Atlantic Oscillation: Climatic Significance and Environmental Impact, Geophys. Monogr.*, Vol. 134, Amer. Geophys. Union, 113–145.

Williams, K., and Coauthors, 2015: The Met Office Global Coupled Model 2.0 (GC2) configuration. *Geosci. Model Dev.*, **8**, 1509–1524, https://doi.org/10.5194/gmd-8-1509-2015.

Williams, R. G., V. Roussenov, D. Smith, and M. S. Lozier, 2014: Decadal evolution of ocean thermal anomalies in the North Atlantic: The effects of Ekman, overturning, and horizontal transport. *J. Climate*, **27**, 698–719, https://doi.org/10.1175/JCLI-D-12-00234.1.

——, ——, M. S. Lozier, and D. Smith, 2015: Mechanisms of heat content and thermocline change in the subtropical and subpolar North Atlantic. *J. Climate*, **28**, 9803–9815, https://doi.org/10.1175/JCLI-D-15-0097.1.

Woollings, T., A. Hannachi, and B. Hoskins, 2010: Variability of the North Atlantic eddy-driven jet stream. *Quart. J. Roy. Meteor. Soc.*, **136**, 856–868, https://doi.org/10.1002/qj.625.

——, C. Czuchnicki, and C. Franzke, 2014: Twentieth century North Atlantic jet variability. *Quart. J. Roy. Meteor. Soc.*, **140**, 783–791, https://doi.org/10.1002/qj.2197.

——, C. Franzke, D. Hodson, B. Dong, E. A. Barnes, C. Raible, and J. Pinto, 2015: Contrasting interannual and multidecadal NAO variability. *Climate Dyn.*, **45**, 539–556, https://doi.org/10.1007/s00382-014-2237-y.

——, L. Papritz, C. Mbengue, and T. Spengler, 2016: Diabatic heating and jet stream shifts: A case study of the 2010 negative North Atlantic Oscillation winter. *Geophys. Res. Lett.*, **43**, 9994–10 002, https://doi.org/10.1002/2016GL070146.

——, and Coauthors, 2018: Daily to decadal modulation of jet variability. *J. Climate*, **31**, 1297–1314, https://doi.org/10.1175/JCLI-D-17-0286.1.

Zhai, X., R. J. Greatbatch, and J. Sheng, 2004: Diagnosing the role of eddies in driving the circulation of the northwest Atlantic Ocean. *Geophys. Res. Lett.*, **31**, L23304, https://doi.org/10.1029/2004GL021146.